SAND2021-14679C

Toward Quantitative Imaging of Soot in an Explosively Generated Fireball

Ashley J. Saltzman*, Daniel R. Guildenbecher†, and Sean P. Kearney‡
Sandia National Laboratories, Albuquerque, NM, 87185, USA

Kevin Wan§, Julien L. Manin**, and Lyle M. Pickett††
Sandia National Laboratories, Livermore, CA, 94550, USA

The detonation of explosives produces luminous fireballs often containing particulates such as carbon soot or remnants of partially reacted explosives. The spatial distribution of these particulates is of great interest for the derivation and validation of models. In this work, three ultra-high-speed imaging techniques: diffuse back-illumination extinction, schlieren, and emission imaging, are utilized to investigate the particulate quantity, spatial distribution, and structure in a small-scale fireball. The measurements show the evolution of the particulate cloud in the fireball, identifying possible emission sources and regions of high optical thickness. Extinction measurements performed at two wavelengths shows that extinction follows the inverse wavelength behavior expected of absorptive particles in the Rayleigh scattering regime. The estimated mass from these extinction measurements shows an average soot yield consistent with previous soot collection experiments. The imaging diagnostics discussed in the current work can provide detailed information on the spatial distribution and concentration of soot, crucial for validation opportunities in the future.

Nomenclature

ΔA = projected pixel area, m^2

I = pixel intensity

I_0 = reference pixel intensity (no absorption)

---

* Postdoctoral Appointee, Engineering Sciences Center, Member AIAA.
† Principal Member of the Technical Staff, Engineering Sciences Center, Senior Member AIAA.
‡ Distinguished Member of the Technical Staff, Engineering Sciences Center, Associate Fellow AIAA.
§ Postdoctoral Appointee, Combustion Research Facility
** Principal Member of the Technical Staff, Combustion Research Facility
††Distinguished Member of the Technical Staff, Combustion Research Facility

k_e = non-dimensional extinction coefficient

KL = optical depth

m = particulate mass, g

λ = wavelength of light, nm

ρ = mass density, kg/m^3

I. Introduction

THE harsh environments created by the detonation of explosives are of great interest for numerous industries, including military, construction, and environmental health and safety. This has driven the need for accurate predictions and models of these events. The products of detonation can produce solid particulates, which may consist of carbon soot and partially reacted explosive material. The emissive properties of these particulates can affect radiative transport within the fireball and may alter reaction rates [1]. In addition, because particulates are assumed to be the dominant source of visible and near infrared emission of the fireball, accurate description of their spatiotemporal distribution is needed for the validation of emission models [2-3].

Research on explosively generated soot has primarily focused on soot production mechanisms very near the primary detonation wave or late time collection and analysis of post-detonation soot often motivated by industrial carbon production. Near the primary detonation wave, previous research has been conducted on primary particle structures and carbon clustering [4]. Time resolved X-ray scattering experiments enabled the investigation of products relative to the time behind the detonation front [5]. Through this work, Watkins et al. [6] have shown rapid carbon cluster growth in locations immediately behind the detonation front, suggesting that a vast majority of the explosive soot is generated early in the detonation. Additionally, Bastea [7] compared chemical equilibrium predictions and experimentally collected carbon content, revealing that equilibrium kinetics freezeout early in the expansion of the detonation products at which point much of the carbon soot has already formed. In other works, which collect and analyze post-detonation soot, nanodiamond production has been studied extensively, emphasizing quantities produced with varying amounts of explosives [8] and the fraction of nanodiamonds in soot [9]. In the interest of quantifying soot production in explosives, Pantea et al. [10] collected particulates over snow and ice and found lower carbon content than in traditional combustion soot.

For more widely studied hydrocarbon combustion flames, soot can be sampled using a probe during the experiment [11]. In contrast, in detonations, the timescales are such that sampling during the fireball generation and development

is extremely challenging. At the same time, the harsh environment produced by the explosion makes it difficult for more complex laser diagnostics to be applied and produce reliable experimental data, especially considering a scaled-up experiment in a larger post-detonation fireball. In contrast, line-of-sight absorption [12] or scattering experiments [13] can be more amenable to these severe settings. By implementing multiple wavelengths to these techniques, variations in optical properties can also be observed [14].

In comparison to soot generated by hydrocarbon combustion, knowledge of the optical properties of explosively generated soot is limited. With the extreme pressure and temperature ranges present in a detonation, explosively generated soot may present unique chemical characteristics, as well as include other particulates such as metallic species or partially reacted explosives [9, 15-16]. Thus, these particulates may have significantly different optical properties, which must be characterized.

From the literature review, it is apparent that little work exists which quantifies the transport, oxidation, and emission of soot within fireballs. The current work seeks to address these gaps by studying explosively generated particulates with ultra-high-speed imaging techniques. In this work, we describe the experiments scrutinizing small-scale fireballs using simultaneous imaging diagnostics including diffuse back-illumination extinction imaging (DBI-EI), schlieren imaging, and emission imaging. A dual wavelength DBI-EI setup is also used as an attempt to characterize the wavelength dependence of the soot absorption properties. Details of the experimental setup are shown in Sect. II. The

II. Experimental Methods

A. Experimental Setup

In the current work, gram-scale experiments are conducted due to their repeatability and relatively low hazards as compared to larger-scale explosive testing. Consequently, these gram-scale experiments are amenable to experimental repetition, which is particularly advantageous for diagnostic development. To generate the fireball, an RP-80 exploding bridgewire detonator (Teledyne RISI) with a standard brass sleeve and no aluminum cup is used. In this device, 80 mg of pentaerythritol tetranitrate (PETN) are first initiated, which then initiates the output pellet consisting of 123 mg of nitramine hexahydro-1,3,5-trinitro-1,3,5-triazine (Royal Demolition Explosive, RDX).

B. Imaging Techniques

A variety of ultra-high-speed imaging techniques are employed in this work to provide a more complete understanding of the fireball structure and particulate distribution. In the first set of experiments, emission and DBI-EI observed the same view, while schlieren imaging observed from the orthogonal perspective. The sensitivity of the schlieren arrangement is adjusted by way of a horizontal knife-edge, providing visualization of the fireball's structure and density gradients. Broadband emission measurements were collected to observe and compare the spatial distribution of primarily emissive or absorptive particles. Preliminary emission and schlieren imaging were reported by Brown et al. [17].

DBI-EI provides the primary quantitative results of the current work. DBI-EI relies on a simple line-of-sight imaging setup consisting of diffuse light passing through the region to measure the optical depth, *KL*, defined by the Beer-Lambert law,

$$KL = -\ln {}^{I}/_{I_0} \tag{1}$$

where *I* is the measured intensity, and I_0 is the reference intensity. As defined by Skeen et al. [14], the mass per pixel integrated along the equivalent optical path length is determined by,

$$m_{soot,pixel} = \rho_{soot} \cdot {}^{\lambda}/_{k_e} \cdot KL \cdot \Delta A_{pixel}, \tag{2}$$

where ρ_{soot} is the soot (particulate) mass density, λ is the wavelength of light, k_e is the non-dimensional extinction coefficient, and ΔA_{pixel} is the projected area of the pixel at the object plane or probe volume. Properties of explosively generated soot, such as the density and extinction coefficient, are not well characterized in the literature and present a challenge for quantifying explosive soot mass in these conditions.

Phase analysis of explosively generated soot has previously found that it is primarily graphitic in structure [18]. Small amounts of nanodiamond, ranging from 10 – 20% by mass, have also been detected in detonation soot by many studies [18 – 20]. As a first estimate, the soot density is approximated as a 20/80 weighted average of diamond and graphite densities, respectively. Using densities from the *Handbook of Chemistry and Physics*, ρ_{soot} was estimated as 2.50 g/cm^3 [21].

Knowledge of the non-dimensional extinction coefficient is essential for deriving the mass from the DBI-EI measurement, as shown by Eq. 2. Within the combustion community, numerous studies have investigated k_e for diesel soot. Skeen et al. [14] have proposed a set of standard k_e values for combustion soot based on extinction measurements

in a flame in the wavelength range of 405 to 850 nm. Due to the lack of literature available for detonation soot, we will utilize those k_e standards for the current work, although this is plainly a source of error for the measurements.

Figure 1 shows the experimental setup around the detonation enclosure. The DBI-EI arrangement utilizes a Cavilux Smart UHS laser (640 nm) for near-uniform illumination of an engineered diffuser behind the detonator. DBI-EI images are observed from an 8%-reflective pellicle beam-splitter, and the camera is equipped with a lens and a 640 ±10 nm bandpass filter to limit detection of the natural luminosity emission from the fireball. Camera frames are arranged in a sequence with alternating laser pulses of different durations: (1) a 0 ns pulse (laser off) to evaluate the fireball emission, (2) 100 ns to observe the less optically dense particulates, and (3) 200 ns to observe the more optically dense particulates. Note that the third frame, with a 200 ns laser pulse, results in a saturated image when no soot is present, but it is used in conjunction with the other two frames to extend the dynamic range of the DBI-EI diagnostic toward high soot concentrations. The broadband emission is observed through the same pellicle beam-splitter by a second camera with a 200-ns exposure time. The emission camera is equipped with a 640-nm notch filter to reject the laser illumination from the DBI-EI system. Lastly, a second Cavilux Smart UHS laser (640 nm, 10 ns pulses) and a knife-edge are used for the schlieren imaging system oriented orthogonal to the other imaging systems. Schlieren images are recorded simultaneously with DBI-EI and emission measurements. All images were recorded using Shimadzu HPV-X2 cameras operating at 2 MHz, recording 128 images per shot for each system.

In a second set of experiments, an additional Cavilux Smart UHS laser (810 nm) was added for preliminary investigation of the soot optical properties and the wavelength dependence of the absorption characteristics. In these dual wavelength DBI-EI experiments, the camera formerly used for broadband emission imaging (Fig. 1c) was instead fitted with an 810 ±10 nm bandpass filter to record the two-dimensional extinction signal at this wavelength. A hot mirror, transmitting 640 nm and reflecting 810 nm light, was used to combine the beams from each Cavilux laser. The schlieren setup was unchanged from Fig. 1.

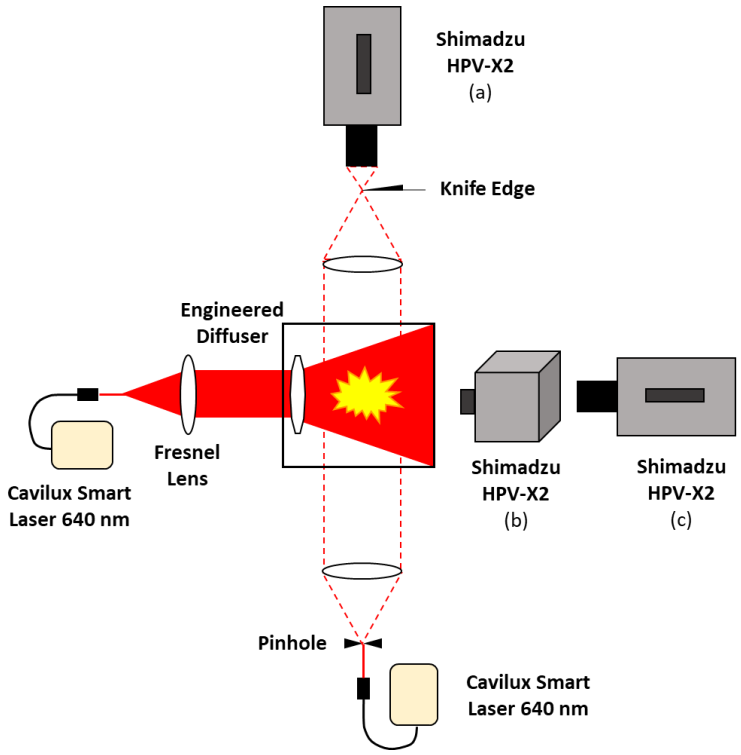

Fig. 1 Setup of the experiment showing the three simultaneous diagnostics. (a) Camera for schlieren imaging. (b) Camera for DBI-EI imaging, fit with 640 nm ± 10 nm bandpass filter. The DBI-EI image is observed through a pellicle mirror (not shown). (c) Camera for broadband emission, fit with 640 nm notch filter.

III.Results and Discussion

This section summarizes the experimental results from the detonation of an RP-80 with a brass sleeve. Simultaneous schlieren, emission, and DBI-EI images were recorded every 0.5 μs, for a duration of 64 μs; however, only select number of frames are shown in the following figures in the interest of brevity and to focus the reported results on the evolution of the fireball with the various diagnostics.

Figure 2 shows sample results of the experiment with the three imaging setups. In the top row, showing schlieren images, the leading shock wave is clearly visible. Dark regions within these frames are presumably caused by particulate absorption in the flow. Note that the schlieren images were recorded orthogonally to the DBI-EI and emission images, so the spatial location of features between these measurements cannot be directly mapped. The second row shows sample images acquired by the broadband emission camera. These images highlight that most of the emission occurs at the head of the fireball, and also that the perceived emission intensity decreases with time. The third row shows the DBI-EI images. The particulates within the fireball are visible and evolve over the duration of the frames shown. A dense particle cloud is evident in the later DBI-EI images.

To aid in identifying emissive particles, the bottom row of Fig. 2. shows the DBI-EI raw images overlayed with false-colored emission images, with brightest intensity shown in red. This row demonstrates that emission primarily originates from regions containing particles following the primary shock. The dense particle cloud shown by DBI-EI does not appear to generate significant emission. This could indicate a much colder region, optical trapping, or that the particles have significantly different optical properties.

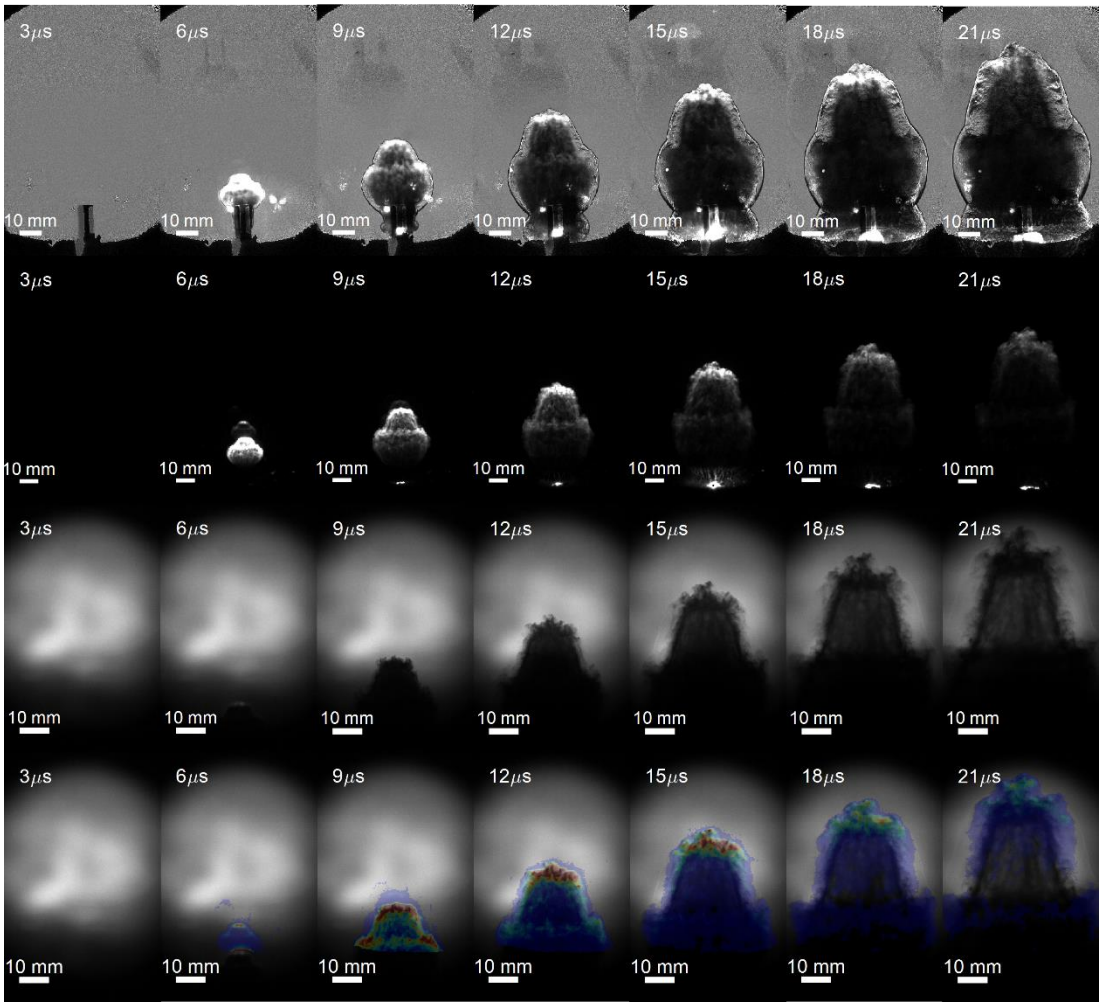

Fig. 2 Selected simultaneous schlieren (top row), emission (second row), and DBI-EI (third row) frames of the fireball from an RP-80 with a brass sleeve and no aluminum cup. Fourth row shows an overlay of the DBI-EI images and emission (false-colored) for clearer mapping of emissive particles.

As previously described, a second set of experiments used an additional DBI-EI system to measure the extinction at a longer illumination wavelength. By analogy to combustion-generated soot, explosively generated soot may have different optical properties at different wavelengths. Prior to the measurements, images were taken of a calibration grid to align the images acquired by the two systems using dewarping and scaling procedures. Figure 3 shows select images from the DBI-EI measurements at two different wavelengths. The physical characteristics of the fireball are

similar to that shown in Fig. 2, albeit with variations in image intensity distribution between the two sets. With the two DBI-EI systems capturing the fireball from the same perspective, the same spatial features can be identified on both sets of images. Visually, both wavelengths show similar amounts of extinction in these raw images, although this will become more apparent in the optical depth comparisons that follow.

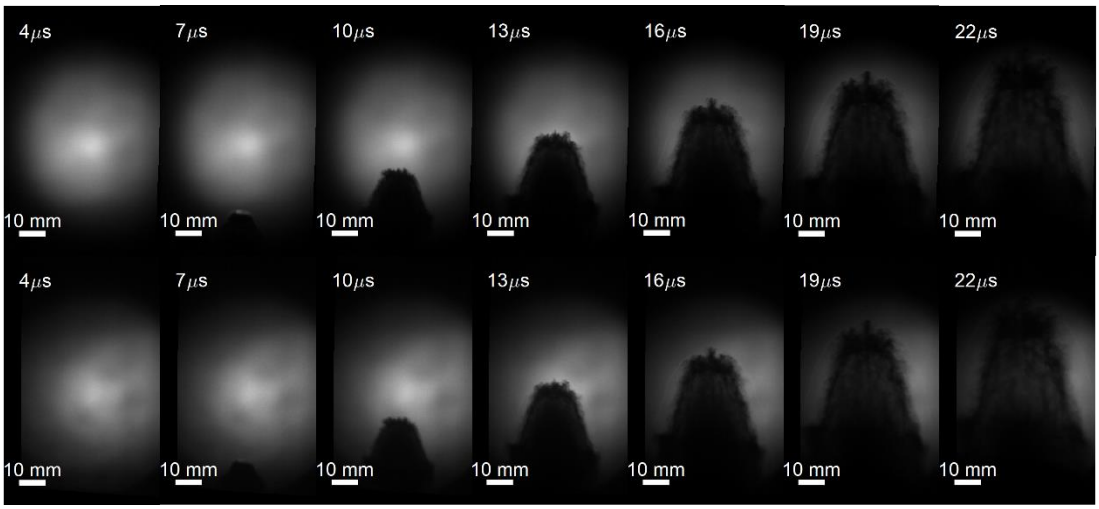

Fig. 3 Images from the two color DBI-EI measurement configuration. Selected frames from 640 nm DBI-EI (top row) and 810 nm DBI-EI (bottom row).

To measure the fireball's extinction using DBI-EI, reference images are taken of the laser pulses prior to the detonation event. Extinction can then be measured relative to the laser intensity in these preshot images using Eq. 1. Figure 3 shows the optical depth of the particulate within the fireball for both the 640 nm and 810 nm illumination wavelengths. Both wavelengths show a region of high optical depth in the lower half of the fireball. A comparably lower, but substantially thick region is also observed near the leading edge of the fireball, which coincides with the significant emission source observed in Fig. 2. The 810 nm wavelength shows slightly lower attenuation than the 640 nm system, as would be expected based on Eq. 2.

The extinction coefficient ratio can be determined experimentally because the soot volume fraction and path length are identical in these simultaneous measurements. The k_e ratio is determined as [14].

$$\frac{(k_e)_{810}}{(k_e)_{640}} = \frac{[KL \cdot \lambda_1]_{810}}{[KL \cdot \lambda_2]_{640}} \tag{3}$$

Where λ_1 is the 810 nm wavelength and λ_2 is the 640 nm wavelength. Using the optical depth measurements, the ratio is calculated and shown in the bottom row of Fig. 4. Throughout the fireball, the k_e ratio is close to unity, meaning KL exhibits a 1/λ dependence, and the extinction coefficient of this soot is roughly independent of wavelength across most

of the soot field. This dependence is consistent with expected behavior of particles in the Rayleigh scattering regime, which are dominated by absorption over scattering [22]. For explosively generated soot, primary particles are on the order of 10 – 50 nm [20, 23]. These length scales are much shorter than the DBI-EI illumination wavelengths used in these experiments, which is again consistent with Rayleigh scattering. Additionally, a near unity k_e ratio has been associated with more mature or annealed soot in sooting flame experiments [12, 24]. This mature soot tends to be more graphitic in morphology and have low hydrogen to carbon ratios [12, 24]. Prior literature has shown that explosively generated soot is highly graphitic, suggesting that these *in situ* extinction measurements are consistent with expectations of graphitic soot [20,23]. One potential exception is the leading tip of the fireball where the measurements reveal higher k_e ratios, which may correspond to nascent or "younger" soot, again, relying on the analogy with combustion-generated soot.

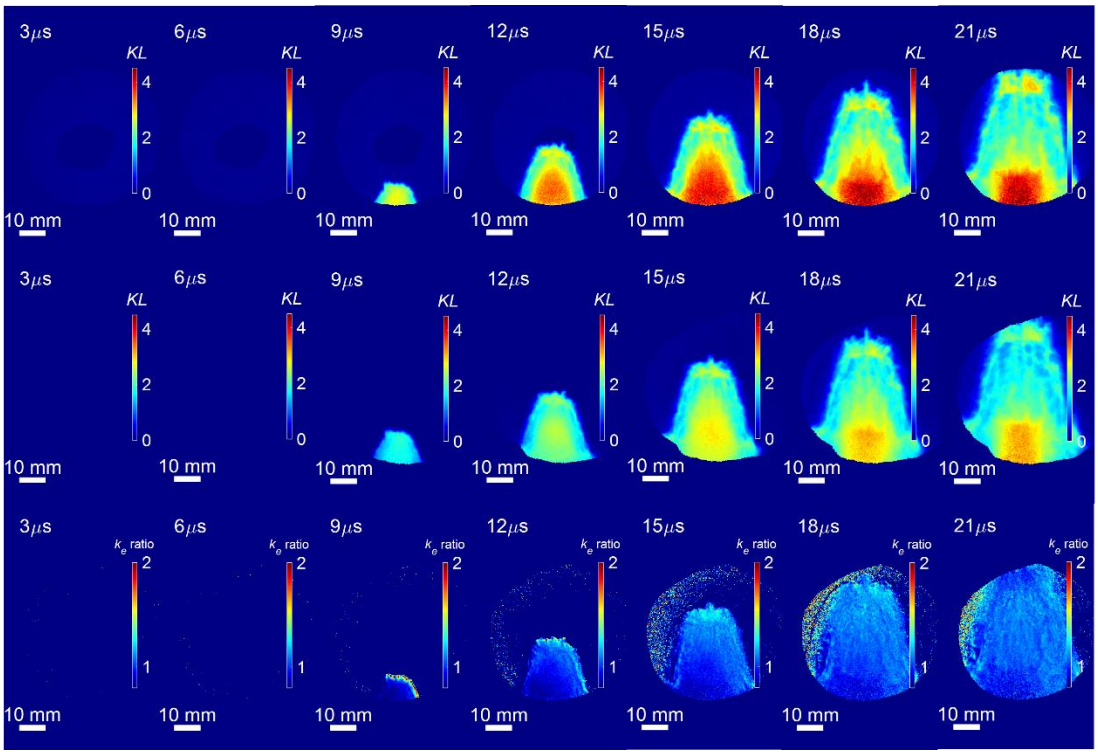

Fig. 4 Optical depth images measured by 640 nm DBI-EI (top row) and 810 nm DBI-EI (middle row), and ratio of the non-dimensional extinction coefficient, 810 nm to 640 nm (bottom row).

Despite the lack of knowledge about optical properties of explosively generated soot, Eq. 2 can be used to estimate the soot mass based on our present knowledge of the previously calculated ρ_{soot} and the proposed standardized k_e values [14]. The total soot yields within the field of view measured via DBI-EI at two wavelengths are plotted as a function of time in Fig. 5. The dashed lines indicate the maximum and minimum masses measured by DBI-EI, based

on four consecutive RP-80 shots, highlighting the repeatability of the experiments. As the k_e ratio was previously found to be close to unity throughout the fireball, a constant k_e of 7.2, evaluated from Skeen et al. [14] near 640 nm, was used for the mass calculation at both wavelengths. Despite the constant dimensionless extinction coefficient and compensating for the longer wavelength, the average mass measured by the 810 nm system is slightly higher than quantified by the 640 nm system. From these combined results, DBI-EI estimates a total yield of 0.95 – 1.13 mol/kg of RDX. Previous literature has determined soot yield based on experimental collections, measuring yields ranging from 2 – 7 mol/kg for RDX [20, 25].

Although the measured extinction-derived mass is lower than these collections from literature, the yield is comparable in order of magnitude. Several sources of error for DBI-EI have previously been mentioned. Primarily, any error in the soot density and extinction coefficient will directly affect the final mass calculation. Additionally, due to the limited field of view of the DBI-EI measurement, any soot outside of the measurement region would not be represented in the total mass calculation. Third, the dynamic range of the cameras fundamentally limits the maximum extinction level, and thus, the mass, that can be reliably measured, since regions of high extinction may lead to intensity measurements that are near or below the noise floor of the camera.

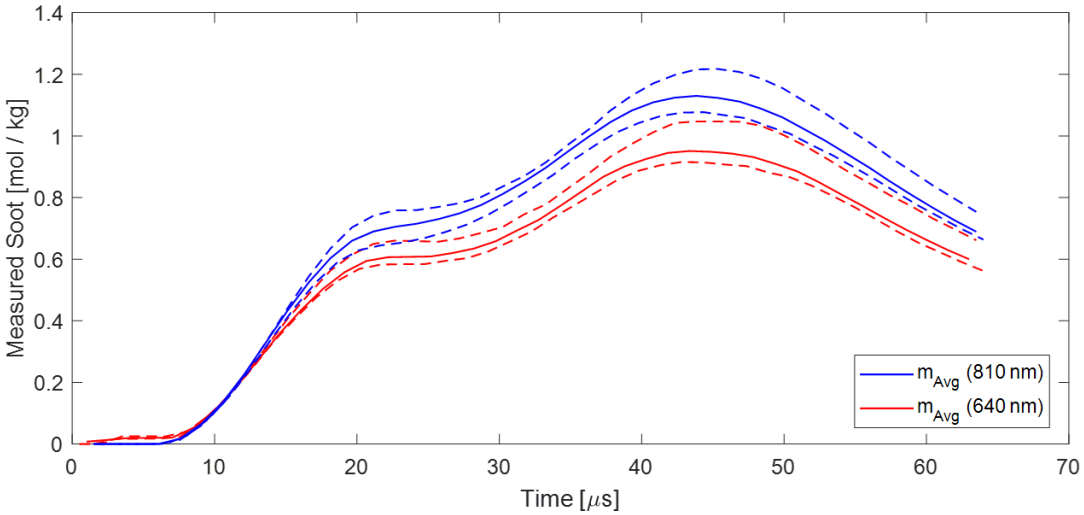

Fig. 5 Measured soot mass within the DBI-EI field of view as a function of time. The regions bound by the dashed lines represent the minimum and maximum mass from four experimental repetitions.

IV. Conclusions

The current work has made significant progress toward the quantification of soot in a post detonation fireball. The fireball was generated by the detonation of a commercially available RP-80 and observed with three in-situ

diagnostics: schlieren, DBI-EI, and broadband emission. The simultaneous diagnostics showed evolution of the fireball, including regions of high absorption by soot particulates. Two laser wavelengths were also utilized in DBI-EI to investigate the wavelength dependence of the detonation soot. The ratio of non-dimensional extinction coefficients was found to be close to unity throughout the fireball. This provides preliminary evidence that the optical properties of detonation soot are dominated by sub-wavelength particles, and that the soot is mature across most of the field. Using the two-dimensional extinction measurements, estimates of total mass were then calculated based on the densities of graphite and diamond, along with extinction coefficients from combustion-generated soot. Despite the known measurement limitations, the mass estimates are comparable to expected yield based on values from the literature.

The diagnostics performed in the current work are expected to enable future quantification of multiple characteristics of post-detonation fireballs and detonation soot. To the authors' knowledge, the current work has shown the first in-situ, time-resolved imaging of explosively generated soot. Better estimates of the properties of explosively generated soot, such as density and dimensionless extinction coefficients, would enable higher fidelity mass measurements in the future. Additional work planned with these diagnostics will assess their repeatability, as well as make comparisons to computations. The information provided by these measurements on the transport and soot concentration in a post-detonation fireball will be vital for future model validation efforts.

Acknowledgments

These experiments would not have been possible without the explosive operations support of Lee Stauffacher, Glenn White, and Sam Reardon. The authors also gratefully acknowledge the support of the Laboratory Directed Research and Development (LDRD) program at Sandia National Laboratories. Sandia National Laboratories is a multi-mission laboratory managed and operated by National Technology and Engineering Solutions of Sandia, LLC., a wholly owned subsidiary of Honeywell International, Inc., for the U.S. Department of Energy's National Nuclear Security Administration under contract DE-NA0003525. The views expressed in the article do not necessarily represent the views of the U.S. Department of Energy or the United States Government.

References

[1] Lebel, L.S., Brousseau, P., Erhardt, L., Andrews, W.S., "Thermochemistry of the combustion of gas phase and condensed phase detonation products in an explosive fireball," *Combustion and Flame*, Vol. 161, No. 4, 2014, pp. 1038-1047. doi: 10.1016/j.combustflame.2013.10.024

[2] Gross, K.C., Wayman, J., and Perram, G.P., "Phenomenological fireball model for remote identification of high-explosives," *Defense and Security Symposium*, Vol. 6566, Orlando, Florida, 2007, pp. 656613-1-12. doi: 10.1117/12.719977

[3] Gross, K.C., Perram, G.P., Tuttle, R.F., "Modeling infrared spectral intensity data from bomb detonations," *Proc. Spie 5811*, Orlando, Florida, 2005, pp. 100-111. doi: 10.1117/12.603206

[4] Firestone, M.A., Dattelbaum, D.M., Podlesak, D.W., Gustavsen, R.L., Huber, R.C., Ringstrand, B.S., Watkins, E.B., Jensen, B., Willey, T., Lauderbauch, L., Hodgin, R., Bagge–Hansen, M., Buuren, T.V., Seifert, S., Graber, T., "Structural evolution of detonation carbon in composition B by X-ray scattering," *AIP Conference Proceedings 1793*, 2017, pp. 030010-1-5. doi: 10.1063/1.4971468

[5] Gustavsen, R.L., Dattelbaum, D.M., Watkins, E.B., Firestone, M.A., Podlesak, D.W., Jensen, B.J., Ringstrand, B.S., Huber, R.C., Mang, J.T., Johnson, C.E., Velizhanin, K.A., Willey, T.M., Hansen, D.W., May, C.M., Hodgin, R.L., Bagge-Hansen, M., Buuren, A.W.v., Lauderbach, L.M., Jones, A.C., Graber, T.J., Sinclair, N., Seifert, S., Gog, T., "Time resolved small angle X-ray scattering experiments performed on detonating explosives at the advanced photon source: Calculation of the time and distance between the detonation front and the x-ray beam," *J Appl Phys*, Vol. 121, No. 10, 2017, pp. 105902-1-10. doi: 10.1063/1.4978036

[6] Watkins, E.B., Velizhanin, K.A., Dattelbaum, D.M., Gustavsen, R.L., Aslam, T.D., Podlesak, D.W., Huber, R.C., Firestone, M.A., Ringstrand, B.S., Willey, T.M., Bagge-Hansen, M., Hodgin, R., Lauderbach, L., van Buuren, T., Sinclair, N., Rigg, P.A., Seifert, S., Gog, T., "Evolution of Carbon Clusters in the Detonation Products of the Triaminotrinitrobenzene (TATB)-Based Explosive PBX 9502," *Journal of Physical Chemistry,* Vol. 121, 201, pp. 23129-23140. doi: 10.1021/acs.jpcc.7b05637

[7] Bastea, S., "Chemical equilibrium and carbon kinetics in explosives," *Proceedings of the 15th International Detonation Symposium,* San Francisco, CA, 2014, p. 896.

[8] Kozyrev, N., Golubeva, E., "Investigation of the synthesis of ultradispersed diamonds in mixtures of TNT with RDX, HMX, and PETN," *Combust Explos Shock Waves*, Vol. 28, 1992, pp. 560-564. doi: 10.1007/BF00755735

[9] Greiner, N.R., Phillips, D.S., Johnson, J.D., and Volk, F., "Diamonds in detonation soot," *Nature*, Vol. 333, 1988, pp. 440-442.

doi: 10.1038/333440a0

[10] Pantea, D., Brochu, S., Thiboutot, S., Ampleman, G., Scholz, G., "A morphological investigation of soot produced by the detonation of munitions," *Chemosphere*, Vol. 65, pp. 821-831.
doi: 10.1016/j.chemosphere.2006.03.027

[11] Michelsen, H.A., "Probing soot formation, chemical and physical evolution, and oxidation: A review of in situ diagnostic techniques and needs," *Proceedings of the Combustion Institute*, Vol. 36, 2017, pp. 717-735.
doi: 10.1016/j.proci.2016.08.027

[12] Williams, T.C., Shaddix, C.R., Jensen, K.A., Suo-Anttila, J.M., "Measurement of the dimensionless extinction coefficient of soot within laminar diffusion flames," *Int. J. Heat Mass Transfer*, Vol. 50, No. 7-8, 2007, pp. 1616-1630
doi: 10.1016/j.ijheatmasstransfer.2006.08.024

[13] Köylü, Ü.Ö. and Faeth, G.M., "Structure of overfire soot in buoyant turbulent diffusion flames at long residence times," *Combustion and Flame*, Vol. 89, No. 2, 1992, pp. 140-156.
doi: 10.1016/0010-2180(92)90024-J

[14] Skeen, S.A., Yasutomi, K., Cenker, E., Adamson, B., Hansen, N., and Pickett, L.M., "Standardized Optical Constants for Soot Quantification in High-Pressure Sprays," *SAE Int. J. Engines*, Vol. 11, No. 6, 2018, pp. 805-816.
doi: 10.4271/2018-01-0233

[15] Abdul-Karim, N., Blackman, C.S., Gill, P.P., Karu, K. "The spatial distribution patterns of condensed phase post-blast explosive residues formed during detonation," *Journal of Hazardous Materials*, Vol. 316, 2016, pp. 204-213.
doi: 10.1016/j.jhazmat.2016.04.081

[16] Abdul-Karim, N., Blackman, C.S., Gill, P.P., Morgan, R.M., Matjacic, L., Webb, R., Ng, W.H., "Morphological Variations of Explosive Residue Particles and Implications for Understanding Detonation Mechanisms," *Journal of Analytical Chemistry*, Vol. 88, No. 7, 2016, pp. 3899-3908.
doi: 10.1021/acs.analchem.6b00080

[17] Brown, A., Son, S.F., Meyer, T.R., Guildenbecher, D.R., "Emission diagnostics for benchtop-scale explosive fireballs," *Laser Applications to Chemical, Security, and Environmental Analysis 2020,* Washington, DC, 2020, 2 pp.

[18] Kuznetzov, V.L., Chuvilin, A.L., Moroz, E.M., Kolomiichuk, V.N., Shaikhutdinov, S.K., Butentko, Y.V., Mal'kov, I.Y., "Effect of explosion conditions on the structure of detonation soots: Ultradisperse diamond and onion carbon," *Carbon,* Vol. 32, No. 5,1994, pp 873-882.
doi: 10.1016/0008-6223(94)90044-2

[19] Titov, V.M., Anisichkin, V.F., Mal'kov, I.Y., "Synthesis of ultradispersed diamond in detonation waves," *Combustion, Explosion and Shock Waves,* Vol. 25, 1989, pp 372-379.

[20] Chen, P. Huang, F. Yun, S., "Characterization of the condensed carbon in detonation soot," *Carbon,* Vol. 41, 2003, pp 2093-2099.

doi: 10.1016/S0008-6223(03)00229-X

[21] "CRC Handbook of Chemistry and Physics," 85th ed., CRC Press, Boca Raton, 2004.

[22] Bohren, C.F., Huffman, D.R., "Absorption and Scattering of Light by Small Particles," 85th ed., Wiley-VCH, Hoboken, NJ, 1998.

[23] Nomura, Y., Kawamura, K., "Soot derived from the detonation of a trinitrotoluene charge," *Carbon,* Vol. 22, No. 2, 1984, pp 189-191.

[24] Michelsen, H.A., Schulz, C., Smallwood, G.J., Will, S., "Laser-induced incandescence: Particulate diagnostics for combustion, atmospheric, and industrial applications," *Prog. Energy Combust. Sci.*, Vol. 51, 2015, pp. 2-48.

doi: 10.1016/j.pecs.2015.07.001

[25] Ornellas, D.L., "Calorimetric Determinations of the Heat and Products of Detonation for Explosives: October 1961 to April 1982," *LLNL Report UCRL-52821,* 1982, 87 pp.